BROADBAND CIRCULARLY POLARIZED DIELECTRIC RESONATOR ANTENNA WITH ANNULAR SLOT EXCITATION

Zheng Zhang[1, *], Xiao-Ming Wang[2], Yong-Chang Jiao[1], and Zi-Bin Weng[1]

[1]National Key Laboratory of Antennas and Microwave Technology, Xidian University, Xi'an, Shanxi 710071, P. R. China

[2]ZTE Corporation, Xi'an, People's Republic of China

Abstract—A broadband circularly polarized (CP) cylindrical dielectric resonator antenna (DRA) is presented. The DRA is excited by an L-shaped microstrip feed line through the coupling of an annular slot in the ground plane. The broadband CP radiation is achieved by using two CP radiators, DRA and annular slot. Broadband impedance match is obtained by introducing an impedance transformer. The optimal configuration offers a 3-dB axial ratio bandwidth of 15.9%, from 6.22 to 7.28 GHz, and a 10-dB impedance bandwidth of 21.3%, from 5.78 to 7.16 GHz. The measured results for the constructed prototype are also exhibited and discussed.

1. INTRODUCTION

Dielectric resonator antenna (DRA) has been widely discussed since it was introduced in 1983 [1]. DRAs offer many advantages, such as low-profile, low-cost, ease of excitation and high radiation efficiency. Extensive studies focused on linear polarization applications, bandwidth enhancing techniques and array applications [2–9]. Recently, much more attention has been paid to circularly polarized (CP) DRAs, including printing a perturbed metal strip on the surface of the dielectric resonator (DR) [10], cross-slot-coupled DRA [11] and dual strips fed DRA [12].

When DRA operates in a fundamental mode, its bandwidth is typically below 10%. Recently, various bandwidth enhancement techniques have been developed for CP DRAs. For single feed

---

excitation, a 10.6% axial ratio (AR) bandwidth has been attained for a stair-shaped rectangular DRA [13], which is excited by a narrow slot rotated at an angle of 45° with respect to the DR side. Another design has been reported in [14], in which a 14% AR bandwidth and 11% impedance bandwidth has been obtained by using an outer-fed square spiral strip. Dual feed excitation is known to generate CP over a broad bandwidth [15–17]. However, in order to provide two quadrature signals, external quadrature couplers should be added in the design.

In this letter, we introduce a broadband circularly polarized cylindrical DRA excited by an L-shaped microstrip feed line through annular slot coupling. The annular slot can resonate near the resonant frequency of the $\text{HEM}_{11\delta}$ mode of the DRA, thus providing greater bandwidth than ordinary dielectric resonator antennas. The feeding mechanism is chosen with the proper parameters to achieve broadband impedance match and good circular polarization characteristic. The simulated results demonstrate that the proposed antenna offers a 3-dB AR bandwidth of 15.9% (6.22–7.28 GHz) and a 10-dB impedance bandwidth of 21.3% (5.78–7.16 GHz). Neither external quadrature feed network nor complex shape of DR are required in this design. The rest of the letter is organized as follows. The antenna geometry and design are presented in Section 2. Experimental results are also provided in Section 3. Conclusions are given in Section 4.

2. ANTENNA GEOMETRY AND DESIGN

Microstrip antenna fed by annular slot coupling to generate CP operation over a wide bandwidth has been presented in [18]. The wideband CP design is achieved by coupling two CP resonant elements, patch and annular slot. For this structure, the slot acts as an aperture coupling feed to excite the patch, as well as a radiator. Based on the work in [18], a broadband CP cylindrical DRA with annular slot excitation is investigated here.

Figure 1 shows the geometry of the proposed antenna. The cylindrical DR has a radius of $a = 5\,\text{mm}$, a height of $d = 12\,\text{mm}$ and a relative permittivity $\varepsilon_d = 10.2$. The DR is positioned on top of the substrate. An annular slot and an L-shaped microstrip feed line are respectively etched on two faces of a rectangular substrate (thickness $h = 1\,\text{mm}$ and relative permittivity $\varepsilon_r = 2.65$) with length $L = 60\,\text{mm}$ and width $W = 60\,\text{mm}$. For the annular slot, the inner radius is R, and the slot width is W_{slot}. The L-shaped feed line is composed of three parts: a $50\,\Omega$ coupling strip (with width $W_{50} = 3\,\text{mm}$), an impedance transformer (with width W_t and length L_t) and an open stub (with
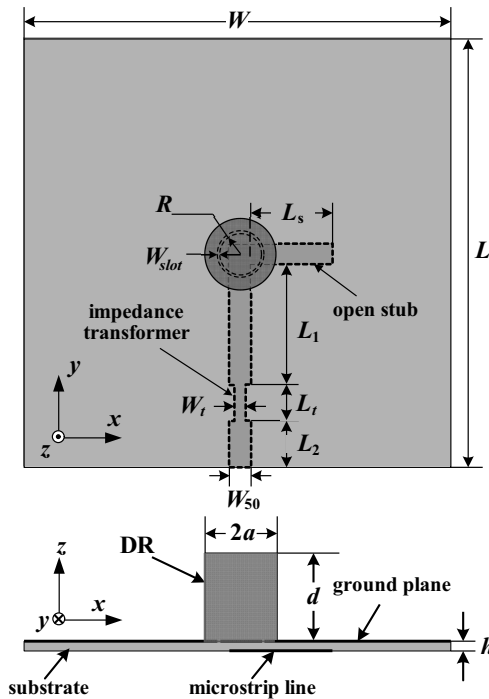
Figure 1. Geometry of the proposed antenna..

width W_{50} and length L_s).

The theoretical resonant frequency of the DRA is calculated by the following equation [2] and is equal to 6.345 GHz ($HEM_{11\delta}$ mode)

$$f_{HEM_{11\delta}} = \frac{c}{2\pi a} \left(\frac{1.6 + 0.513x + 1.392x^2 - 0.575x^3 + 0.088x^4}{\varepsilon_d^{-0.42}} \right) \quad (1)$$

where $x = a/2d$ and c is the speed of light in free space.

The resonant frequency of the annular slot can be approximately expressed as

$$f_{slot} \approx \frac{c}{2\pi \left(R + w_{slot}/2 \right) \sqrt{\varepsilon_{eff}}} \quad (2)$$

where ε_{eff} can be calculated by

$$\varepsilon_{eff} = \frac{(\varepsilon_r + \varepsilon_d)}{2} \quad (3)$$

First, we investigate the resonant frequency of the annular slot. Here, the simulations are performed using Ansoft HFSS ver.11 [19],

a commercially available 3-D electromagnetic field solver based on the finite element method (FEM). Fig. 2 plots the simulated return losses for different values of R (without impedance transformer). The calculated and simulated resonant frequencies of the annular slot with different values of R are summarized in Table 1. The simulated results are close to the calculated ones, except for $R = 2.7$ mm. When R equals to 2.7 mm, the calculated resonant frequency of the slot is close to the DRA's, which makes it different from the calculated one. The resonant frequencies of DRA are not distinct in Fig. 2. However, the return losses are close to 10 dB at 6.4 GHz, which corresponding to the resonant frequency of DRA.
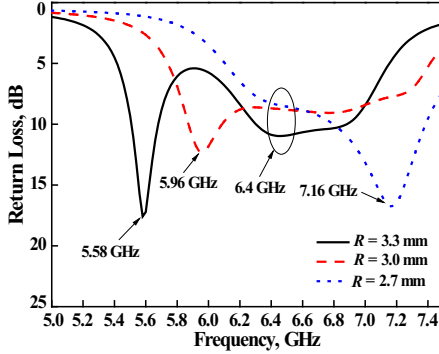
Figure 2. Simulated return losses for different values of R, with $L_s = 11.5$ mm, $L_1 = 17$ mm, $L_2 = 6.5$ mm, $L_t = 5$ mm, $W_{slot} = 0.25$ mm, and $W_t = W_{50} = 3$ mm.

Table 1. Calculated and simulated resonant frequencies of the slot mode.

R	Calculated	Simulated
2.7 mm	6.67 GHz	7.16 GHz
3.0 mm	6.03 GHz	5.96 GHz
3.3 mm	5.50 GHz	5.58 GHz

Figure 3 plots the simulated AR curves for different values of R. It is observed that two of the curves contain two CP operating frequencies. The lower frequency is almost constant; however, the higher frequency is decreased with increasing R. Hence, the higher and lower CP frequencies could be due to the annular slot mode and two orthogonal $HEM_{11\delta}$ modes of DRA, respectively. It should be

noted that the CP operating frequencies are not consistent with the resonant frequencies. According to the studies in [20] and [21], the CP operating frequencies are much related to the length, L_s, of the open stub. The improper length of the open stub would cause the amplitude and phase errors of two orthogonal modes, resulting in an increased AR. When the values of R and L_S are chosen properly, the two radiating elements can have good CP performances at the same time. As shown in Fig. 4, a broad AR bandwidth is obtained when $L_s = 11.5$ mm and $R = 3$ mm. The DRA exhibits a simulated 3-dB AR bandwidth of 15.9%, from 6.22 to 7.28 GHz, by merging two separate CP frequencies. In our simulation work, a broad AR bandwidth could also be achieved when L_s equals to 24 mm; however, it is not suitable for array applications.
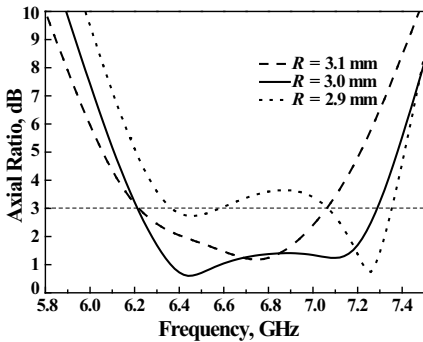
Figure 3. Simulated AR curves for different values of R, with $L_s = 11.5$ mm, $L_1 = 17$ mm, $L_2 = 6.5$ mm, $L_t = 5$ mm, $W_{slot} = 0.25$ mm, and $W_t = W_{50} = 3$ mm.
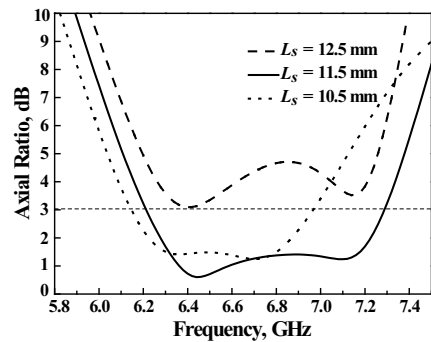
Figure 4. Simulated ARs for different values of L_s, with $L_1 = 17$ mm, $L_2 = 6.5$ mm, $L_t = 5$ mm, $R = 3$ mm, $W_{slot} = 0.25$ mm, and $W_t = W_{50} = 3$ mm.

In addition, an impedance transformer is introduced to improve the impedance bandwidth. The simulated return loss, AR and input impedance curves of the DRA with or without the impedance transformer are plotted in Fig. 5. It can be seen that the introduced impedance transformer has little effect on the AR bandwidth, but it affects the impedance bandwidth soundly. By properly choosing the dimension of the impedance transformer, the DRA exhibits a simulated 10-dB impedance bandwidth of 21.3%, from 5.78 to 7.16 GHz.

To gain further understanding of the way LHCP is excited, we also examine the electric field distribution of 0°, 90°, 270° and 360°
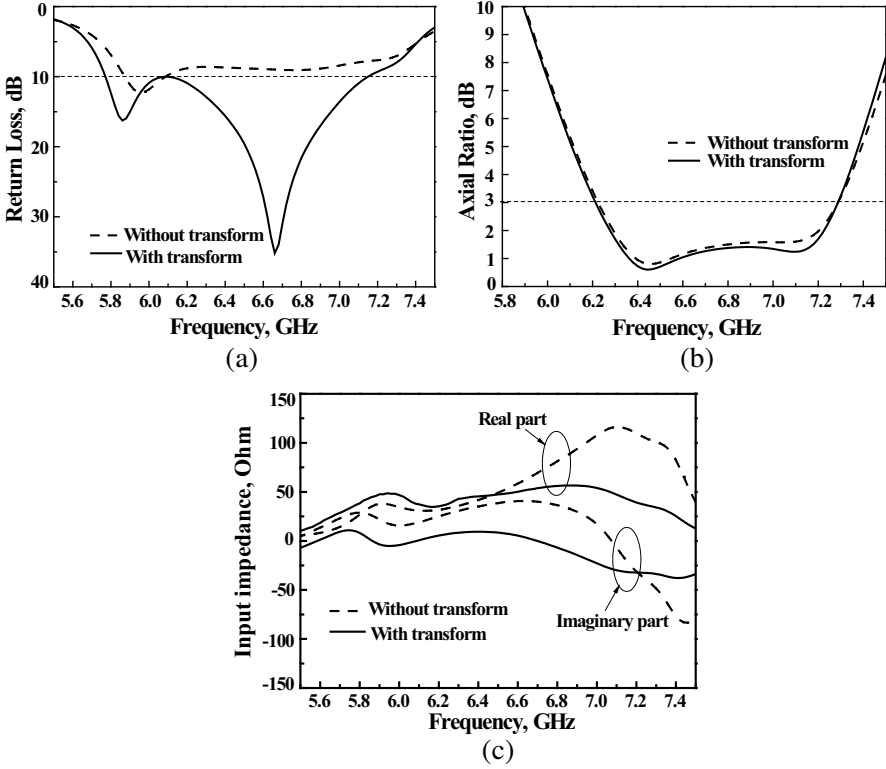
Figure 5. (a) Simulated return losses versus frequency with or without the transformer. (b) The corresponding ARs versus frequency with or without the transformer. (c) Simulated input impedance versus frequency with or without the transformer. ($L_s = 11.5$ mm, $L_1 = 17$ mm, $L_2 = 6.5$ mm, $L_t = 5$ mm, $R = 3$ mm, $W_{slot} = 0.25$ mm, and $W_t = 1.5$ mm).

on the proposed DRA. The vectors of the E-field on the annular slot of the DRA at the resonate frequency 6.64 GHz is shown in Fig. 6. Since the direction of wave propagation is along the $+z$ direction, it can be easily observed that the proposed DRA can generate LHCP radiations. Fig. 7 presents the E-field distribution in the cylindrical DR in two orthogonal planes at the resonate frequency 6.64 GHz. Note that at the resonant frequency, two orthogonal $HEM_{11\delta}$ modes, with almost equal amplitude and a 90° phase difference, concurred in the DR. It is demonstrated that the proposed antenna can radiate a fairly good CP waves at the resonate frequency.
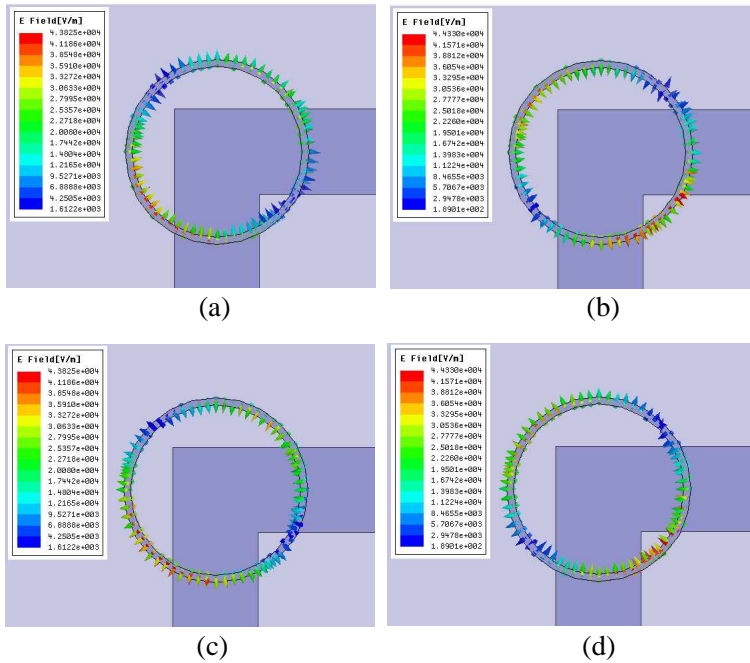
Figure 6. The vectors of the E-field on the annular slot of the DRA at 6.64 GHz. (a) 0°. (b) 90°. (c) 180°. (b) 270°.
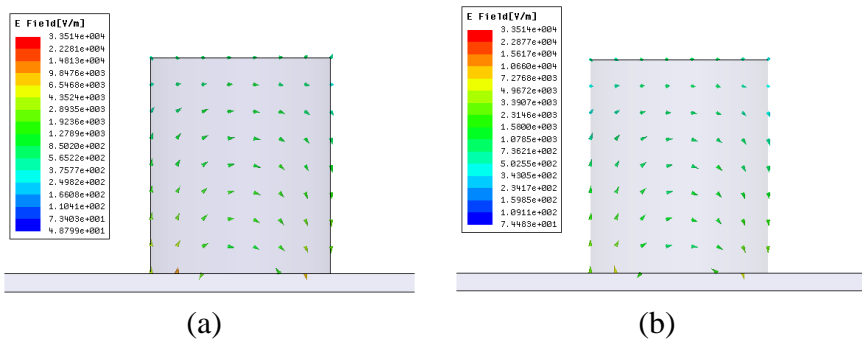
Figure 7. The vectors of the E-field in the cylindrical DR at 6.64 GHz. (a) xoz plane (0°). (b) yoz plane (90°).

3. RESULTS AND DISCUSSION

A prototype of the optimized antenna was fabricated and tested, with the photography shown in Fig. 8. The DR was fabricated with a

ceramic material of relative permittivity 10.2. The optimal dimensions of the feed line are: $L_s = 11.5\,\text{mm}$, $L_1 = 17\,\text{mm}$, $L_2 = 6.5\,\text{mm}$, $L_t = 5\,\text{mm}$, $R = 3\,\text{mm}$, $W_{slot} = 0.25\,\text{mm}$ and $W_t = 1.5\,\text{mm}$. The prototype has been measured using WILTRON37269A vector network analyzer and the anechoic chamber. Some representative measured results along with some simulated data are presented.

(a)   (b)
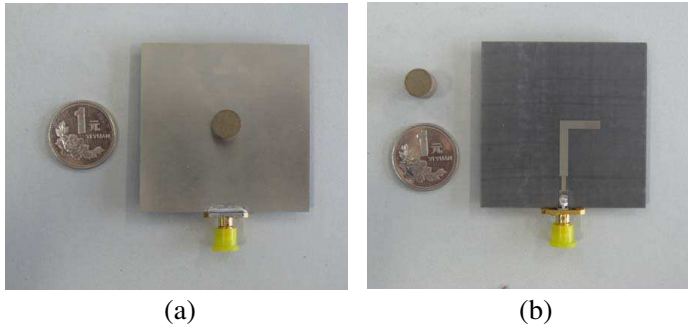
Figure 8. Photography of the antenna prototype. (a) Front view. (b) Rear view.

The measured and simulated return losses are displayed in Fig. 9. The measured 10-dB return loss achieves an impedance bandwidth of about 20.7% (5.85–7.20 GHz), and the simulated impedance bandwidth is about 21.3% (5.78–7.16 GHz). Due to the fabrication tolerance of the DR, the effective relative permittivity of the DR is lower than
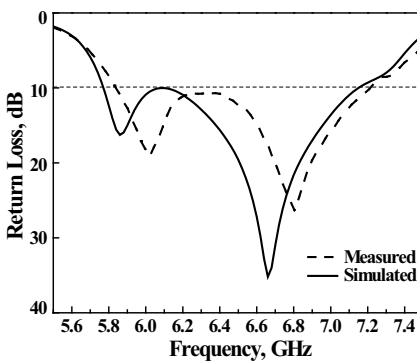
Figure 9. Measured and simulated return losses of the proposed antenna.
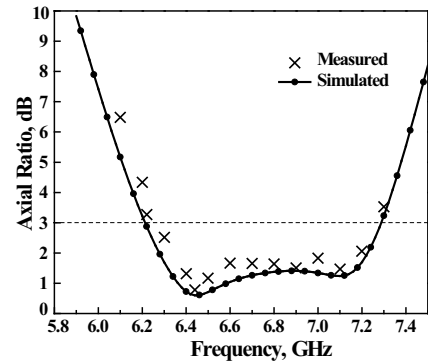
Figure 10. Measured and simulated ARs versus frequency at boresight direction.

10.2, which results in higher resonant frequencies compared with the simulated results. In spite of this difference, there is a good agreement between the measured and simulated results. As shown in Fig. 10, the
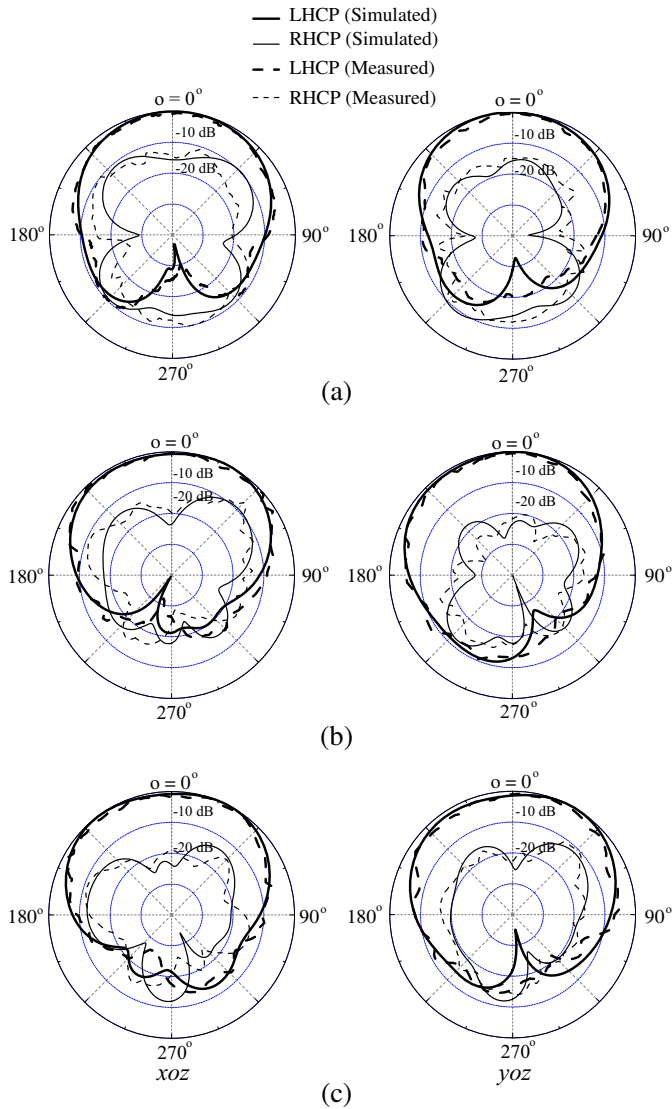
Figure 11. Measured and simulated normalized radiation patterns of the proposed antenna at different frequencies. (a) 6.22 GHz. (b) 6.7 GHz. (c) 7.1 GHz.

measured 3-dB AR bandwidth is about 14.6% (6.22–7.20 GHz), while
the simulated 3-dB AR bandwidth is about 15.9% (6.22–7.28 GHz).
It should be mentioned that the entire measured AR passband falls
within the impedance passband, which is highly desirable.

Figure 11 plots the measured and simulated normalized radiation
patterns in two orthogonal cuts at 6.22 GHz, 6.7 GHz and 7.1 GHz,
respectively.   In each radiation pattern, the left-hand circularly
polarized (LHCP) field is more than 15 dB stronger than the right-hand
circularly polarized (RHCP) in the boresight direction ($\theta = 0°$). Fig. 12
presents the measured and simulated gains of the proposed antenna,
where the measured peak gain varies between 4.15 and 6.09 dBi across
the measured 3-dB AR bandwidth (6.22–7.20 GHz). Fig. 13 shows the
simulated radiation efficiency of the proposed antenna. It is observed
that the radiation efficiency is higher than 95% from 6.18 to 7.16 GHz,
which demonstrates high radiation efficiency of the DRA.
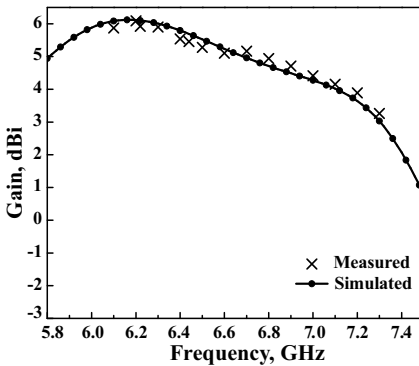
Figure 12. Measured and
simulated gains of the proposed
antenna.
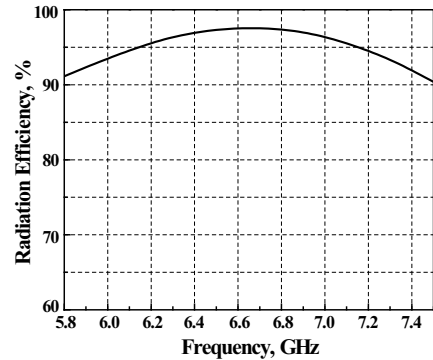
Figure 13. Simulated radia-
tion efficiency of the proposed an-
tenna.

The proposed DRA is compared with antennas in [9, 13–15], their
respective performances are tabulated in Table 2. As can be seen
from the first three rows of Table 2, the proposed antenna exhibits the
widest 3-dB axial ratio bandwidth among the quoted antennas. For the
antenna in the fourth row, though the 3-dB axial ratio bandwidth is
wider than the proposed antenna, external quadrature couplers should
be added in the design, which increase the complexity and the size of
the design.

Table 2. Comparison with other designs.

Ref.	Implementation methods	10-dB impedance bandwidth	3-dB axial ratio bandwidth
[9]	stepped impedance microstrip feed line/ trapezoidal-shaped resonator	4.21~10.72 GHz (87.3%)	5.17~5.88 GHz (12.85%)
[13]	narrow rectangular slot/ rectangular stair shaped DRA (rotated 45°)	7.56~10.95 GHz (36.6%)	9.3~10.3 GHz (10.2%)
[14]	outer-fed square spiral strip/ rectangular DRA	11%	14%
[15]	a pair of 90° hybrid couplers/ cylindrical DRA	1.75~2.48 GHz (34.5%)	1.65~2.14 GHz (25.9%)
This work	L-shaped microstrip feed line/ cylindrical DRA and annular slot as two CP radiators	5.78~7.16 GHz (21.3%)	6.22~7.28 GHz (15.9%)

4. CONCLUSION

A broadband CP DRA design has been proposed and implemented. By merging the bands of two modes, slot mode and $HEM_{11\delta}$ mode, the proposed antenna achieves a simulated AR bandwidth of 15.9% from 6.22 to 7.28 GHz. By introducing an impedance transformer, the simulated 10-dB impedance bandwidth reaches to 21.3% from 5.78 to 7.16 GHz. The experimental results are in good agreement with the simulated results. The entire measured AR passband falls within the impedance passband. In addition, this antenna also provides a stable broadside radiation with a gain range from 4.15 to 6.09 dBi in the operating bandwidth.

REFERENCES

1. Long, S. A., M. W. McAllister, and L. C. Shen, "The resonant cylindrical dielectric cavity antenna," *IEEE Trans. Antennas Propag.*, Vol. 31, No. 3, 406–412, May 1983.

2. Luk, K. M. and K. W. Leung, *Dielectric Resonator Antennas*, Research Studies Press Ltd., Hertfordshire, UK, 2003.

3. Zainud-Deen, S. H., H. A. El-Azem Malhat, and K. H. Awadalla, "A single-feed cylindrical superquadric dielectric resonator antenna for circular polarization," *Progress In Electromagnetics Research*, Vol. 85, 409–424, 2008.

4. Kumar, A. V. P., V. Hamsakutty, J. Yohannan, and K. T. Mathew, "Microstripline fed cylindrical dielectric resonator antenna with a coplanar parasitic strip," *Progress In Electromagnetics Research*, Vol. 60, 143–152, 2006.

5. Saed, M. A. and R. Yadla, "Microstrip-fed low profile and compact dielectric resonator antennas," *Progress In Electromagnetics Research*, Vol. 56, 151–162, 2006.

6. Zainud-Deen, S. H., H. A. El-Azem Malhat, and K. H. Awadalla, "A single-feed cylindrical superquadric dielectric resonator antenna for circular polarization," *Progress In Electromagnetics Research*, Vol. 85, 409–424, 2008.

7. Wee, F. H., M. F. B. A. Malek, S. Sreekantan, A. U. Al-Amani, F. Ghani, and K. Y. You, "Investigation of the characteristics of Barium Strontium Titanate (BST) dielectric resonator ceramic loaded on array antenna," *Progress In Electromagnetics Research*, Vol. 121, 181–213, 2011.

8. Abdulla, P. and A. Chakraborty, "Rectangular waveguide-fed hemispherical dielectric resonator antenna," *Progress In Electromagnetics Research*, Vol. 83, 225–244, 2008.

9. Danesh, S., S. K. Abdul Rahim, and M. Khalily, "A wideband trapezoidal dielectric resonator antenna with circular polarization," *Progress In Electromagnetics Research Letters*, Vol. 34, 91–100, 2012.

10. Leung, K. W. and H. K. Ng, "Theory and experiment of circularly polarized dielectric resonator antenna with a parasitic patch," *IEEE Trans. Antennas Propag.*, Vol. 31, No. 3, 406–412, May 1983.

11. Huang, C. Y., J. Y. Wu, and K. L. Wong, "Cross-slot-coupled microstrip antenna and dielectric resonator antenna for circular polarization," *IEEE Trans. Antennas Propag.*, Vol. 47, No. 4, 605–609, April 1999.

12. Leung, K. W., W. C. Wong, K. M. Luk, and E. K. N. Yung, "Circular-polarised dielectric resonator antenna excited by dual conformal strips," *Electron. Lett.*, Vol. 36, No. 6, 484–486, March 2000.

13. Chair, R., S. L. S. Yang, A. A. Kishk, K. F. Lee, and K. M. Luk, "Aperture fed wideband circularly polarized rectangular stair shaped dielectric resonator antenna," *IEEE Trans. Antennas Propag.*, Vol. 54, No. 4, April 2006.

14. Sulaiman, M. I. and S. K. Khamas, "A singly fed rectangular dielectric resonator antenna with a wideband circular polarization," *IEEE Antennas Wireless Propag. Lett.*, Vol. 9, 615–618, 2010.

15. Khoo, K. W., Y. X. Guo, and L. C. Ong, "Wideband circularly polarized dielectric resonator antenna," *IEEE Trans. Antennas Propag.*, Vol. 55, No. 7, 1929–1932, July 2007.

16. Massie, G., M. Caillet, M. Clenet, and Y. M. M. Antar, "A new wideband circularly polarized hybrid dielectric resonator antenna," *IEEE Antennas Wireless Propag. Lett.*, Vol. 9, 347–350, 2010.

17. Yang, S. S., R. Chair, A. A. Kishk, K. F. Lee, and K. M. Luk, "Study on sequential feeding networks for subarrays of circularly polarized elliptical dielectric resonator antenna," *IEEE Trans. Antennas Propag.*, Vol. 55, No. 2, 321–333, Feb. 2007.

18. Su, C. W. and J. S. Row, "Slot-coupled microstrip antenna for broadband circular polarization," *Electron. Lett.*, Vol. 42, No. 6, 318–319, 2006.

19. Ansoft High Frequency Structure Simulator (HFSS), Ver. 11.0, Ansoft Corp., 2007.

20. Row, J. S., "Design of aperture-coupled annular-ring microstrip antennas for circular polarization," *IEEE Trans. Antennas Propag.*, Vol. 53, No. 5, 1779–1784, 2005.

21. Row, J. S., "The design of a square-ring slot antenna for circular polarization," *IEEE Trans. Antennas Propag.*, Vol. 53, No. 5, 1967–1972, 2005.